Vehicular and Core-Shell Nanoparticle Diffusion in Attractive Entangled Polymer Melts

Kaitlin Wang[1] and **Karen I. Winey**[1,2,*]

[1] Department of Materials Science and Engineering, University of Pennsylvania, Philadelphia, PA 19104, United States of America

[2] Department of Chemical and Biomolecular Engineering, University of Pennsylvania, Philadelphia, PA 19104, United States of America

***Corresponding author:** Karen I. Winey, winey@seas.upenn.edu,

Address: Laboratory for Research on the Structure of Matter, 3231 Walnut St, Philadelphia, PA 19104

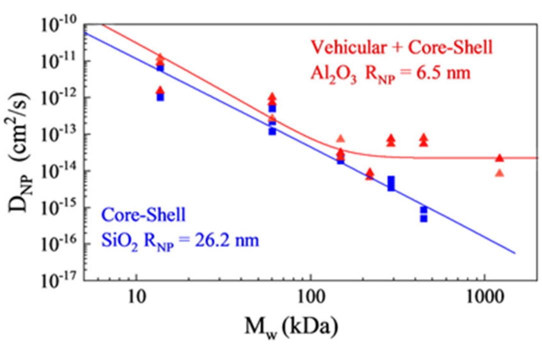

For Table of Contents Use only

Abstract

This work studies nanoparticle (NP) diffusion in attractive polymer melts and reveals two distinct dynamic modes: vehicular and core-shell. By diffusing alumina NPs (R_{NP} = 6.5 nm) and silica NPs (R_{NP} = 8.3 and 26.2 nm) into poly(2-vinylpyridine) melts of various molecular weights (14 - 1220 kDa), we examine the impact of the R_{NP}, polymer size (R_g), and surface chemistry on NP diffusion. Using time-of-flight secondary ion mass spectrometry and trilayer samples, we measure cross-sectional nanoparticle concentration profiles as a function of annealing time and extract nanoparticle diffusion coefficients. Both small and large silica NPs (R_g/R_{NP} = 0.12 – 3.6) display core-shell behavior, while alumina NPs (R_g/R_{NP} = 0.50 – 4.6) diverge sharply with increasing polymer molecular weight, aligning with theoretically predicted vehicular diffusion. The transition from core-shell to vehicular diffusion is the result of both increasing molecular weight and weaker nanoparticle/polymer attractions and facilitates an estimate of the monomer desorption time.

Keywords: Polymer nanocomposites, nanoparticle diffusion, molecular weight, ToF-SIMS

Introduction

Polymer nanocomposites (PNCs) have garnered considerable interest as advanced materials, due to their tunable properties. Introducing nanoparticles (NPs) into a polymer matrix permits nuanced adjustments to optimize mechanical, thermal, electrical, and optical attributes to meet specific performance criteria. This adaptability positions PNCs as a promising material class across diverse sectors including electronics, aerospace, automotive, and biomedical industries.[1–4]

Previous work has clearly established that the spatial distribution of NPs significantly impacts processability and properties, including mechanical properties, rheology, and gas permeability within PNCs.[5–8] To achieve and maintain the desired properties, understanding and predicting nanoparticle diffusion is critically important. Factors such as NP size, NP shape, NP concentration, and the interaction between polymer and NPs must be managed to achieve desired NP distributions and properties for effective PNC applications.[9–11] PNCs with strong attractions between the NPs and polymer matrix are distinguished by improved NP dispersion and maintain industrially relevant processability advantages compared to their neutral counterparts. Thus, NP diffusion behavior in these attractive nanocomposites is of particular interest and a crucial cornerstone for PNC applications.[12]

When particles are microscopic, particle diffusion in a viscous medium is well described by Stokes-Einstein (SE) behavior, $D_{SE} = \frac{k_B T}{6\pi\eta R}$. However, significant deviations have been reported for nanoparticle diffusion, particularly in the presence of attractive polymer-nanoparticle interactions.[13–19] Nanoparticle diffusion studies in neutral melts have also highlighted substantial deviations from SE, depending on the NP radius and polymer tube diameter, d_T.[18,20,21] In athermal systems, spherical nanoparticles with diameters larger than d_T exhibit a hopping diffusion mechanism in which the NPs overcome topological energy barriers to move faster than Stokes-

Einstein predictions.[22] Small nanoparticles, due to their size being comparable to or smaller than the polymer's mesh size, exhibit diffusion rates largely unaffected by the surrounding polymer.[23] Within attractive melts, Schweizer's group introduced two simultaneous NP diffusion modes—the core-shell and vehicle modes—where the relative time scales of polymer and NP dynamics dictate the dominant mode.[16,17] The total diffusion coefficient of a nanoparticle is described by the sum of the core-shell and vehicle modes.

$$D_{NP,theory} = D_{core\text{-}shell} + D_{vehicle} \tag{1}$$

The core-shell contribution follows the SE behavior and accounts for 1) the viscosity of the PNC rather than the neat polymer and 2) the effective nanoparticle size rather than the bare NP size due to a bound polymer layer,

$$D_{core-shell} = \frac{k_B T}{6\pi \eta_{PNC} R_{eff}} \tag{2}$$

where k_B is the Boltzmann constant, T is the annealing temperature in Kelvin, η_{PNC} is the PNC viscosity in Pa·s, and the effective nanoparticle radius is $R_{eff} = R_{NP} + R_g$. These modifications to SE behavior result in slower NP diffusion. A variety of experimental methods have be used to measure diffusion coefficients of nanoparticles in polymer melts include Rutherford backscattering (RBS) (R_{NP} = 13 nm),[14,24] dynamic light scattering (DLS) (R_{NP} = 0.88, 5 nm),[17] and single particle tracking (SPT) (R_{NP} = 6.5-6.6 nm) .[25] The core-shell mechanism (Eqn. 2) alone has been sufficient to understand NP diffusion in various experimental systems with strong polymer-nanoparticle interactions: unentangled poly(propylene glycol) (PPG) melts with octaamino-phenylsilsesquioxane (OAPS) nanoparticles,[17] PPG with small silica (SiO_2) NPs,[17] and poly(2-vinly pyridine) (P2VP) with SiO_2 NPs.[14] In addition, there are examples of $D_{NP} < D_{SE}$ in poly(ethylene oxide) with SiO_2 NPs,[26] and PPG with strongly interacting quantum dot samples through COOH surface functionalization.[27] These systems represent a wide range of R_g/R_{NP} (~0.1

to 1.2), and the core-shell model well explains the decrease in D_{NP} compared to Stokes-Einstein behavior.

The vehicular mode for NP diffusion involves polymer desorption and results in diffusion coefficients faster than SE behavior when the desorption of the polymer is faster than the polymer chain dynamics. This mechanism is described by using four polymer time scales: τ_{des} – monomer desorption time, τ_e – entanglement onset time, τ_{Rouse} – longest chain Rouse relaxation time, and τ_{rep} – reptation time.[16] In Regime I, the monomer desorption time is relatively quick, meaning shorter than the entanglement onset time ($\tau_{des} < \tau_e$). In this regime the vehicular contribution to $D_{NP,theory}$ scales as ~ τ_{des}^{-1} as

$$D_{vehicle-I} = Ab \times \frac{D_0}{\tau_{des}} \tag{3}$$

where A is a numerical prefactor, b is the Kuhn monomer length, and D_0 is the segmental diffusion constant. In this study, Regime I will be neglected because the nanoparticles have surface hydroxyl groups that interact favorably with the polymer, such that τ_{des} is expected to be longer than τ_e. In Regime II, the desorption time is longer than the entanglement onset time and shorter than the Rouse time ($\tau_e < \tau_{des} < \tau_{Rouse}$), indicating an intermediately strong NP-polymer attraction, such that the vehicular contribution to NP diffusion scales ~ $1/\tau_{des}^{3/4}$ as

$$D_{vehicle-II} = Ad_T(b^2D_0)^{\frac{1}{4}} \times \left(\frac{1}{\tau_{\mathrm{des}}}\right)^{\frac{3}{4}} \tag{4}$$

where d_T is the tube diameter. At slower desorption times, although still faster than polymer reptation ($\tau_R < \tau_{des} < \tau_{rep}$), the vehicular contribution to NP diffusion in Regime III has a molecular weight dependence,

$$D_{vehicle-III} = Ad_T\left(\frac{D_0}{N\tau_{des}}\right)^{\frac{1}{2}} \tag{5}$$

where N is the degree of polymerization. Regime III is the only case in which $D_{vehicle}$ depends on both the desorption time and the polymer molecular weight with a scaling dependence of $(N\tau_{des})^{-1/2}$. To date, the experimental systems that suggest a vehicular mechanism for NP diffusion have used very small nanoparticles (R_{NP} < 1 nm). Specifically, nanocomposites of PPG with OAPS and P2VP with OAPS exhibit fast NP diffusion relative to the core-shell model.[17,13]

In this manuscript, we experimentally identify PNCs with NP diffusion controlled by both the core-shell and the vehicular modes. Leveraging the capabilities of our previously demonstrated time-of-flight secondary ion mass spectrometry (ToF-SIMS) method,[28] we accurately measure NP diffusion coefficients on micron length scales and across a considerable range, D_{NP} = 10^{-18} – 10^{-11} cm^2/s. By employing a wide range of P2VP molecular weights (14 – 1220 kg/mol) and three NPs that vary in size and surface chemistry, we reveal systems dominated by core-shell and by vehicle NP diffusion. Finally, we discuss the implications of these distinct diffusion modes and estimate desorption times (τ_{des}) of the bound layer.

Experimental Methods

Materials: Poly(2-vinylpyridine) (P2VP) of weight averaged molecular weights 14.0, 41.0, 158, 219, 310, 474, and 1220 kDa (narrow distribution, PDI <1.10) were purchased from Scientific Polymer Products Inc. and used as-received. Gel permeation chromatography (GPC) was used to measure the polymers' molecular weights and respective PDIs (**Table S1**). Nissan-STL silica (SiO_2) nanoparticles were solvent-exchanged from methyl-ethyl ketone (MEK) to methanol (MeOH) via crashing the particles out of MEK.[28] Aluminum oxide (Al_2O_3) NPs were purchased from Sigma Aldrich, then suspended in a 50 g/L MeOH solution, vortexed for 1 min, sonicated for > 30 min, and filtered through 1 μm and 0.2 μm filters subsequently. A small amount of the respective molecular weight P2VP (5 g/L) was added to the MeOH-Al_2O_3 solution to form a bound layer on the bare NPs to prevent subsequent aggregation. The solution was stirred constantly, and excess MeOH was evaporated to achieve the desired NP vol % after filtration. Ludox silica nanoparticles are solvent exchanged from water to ethanol through creating a miscible water/ethanol solution, then adding concentrated P2VP/ethanol solution. The solution is then diluted with ethanol to the desired concentration. Nanoparticle sizes and size dispersities were determined using small-angle X-ray scattering (SAXS) on a capillary filled with a dilute NP suspension and fit using the hard sphere model. The Nissan SiO_2 NPs fit to hard sphere resulted in R_{NP} = 26.1 nm, PDI 1.19, and the Ludox SiO_2 NPs measured R_{NP} = 8.3 nm, PDI 1.15. Aluminum oxide (Al_2O_3) NPs measured R_{NP} = 6.5 ± 2.5 nm, PDI = 1.14, with dynamic light scattering (DLS) measuring hydrodynamic diameter consistent with ~ R_{NP} +R_g. Silicon wafers (<100>) with a thick thermal oxide layer (referred to as SiO_2 wafers hereafter) were purchased from Nova Electronic Materials. Silicon wafers (<100>) (Si wafer) were purchased from Wafer World Inc.

<u>Trilayer Fabrication and Nanoparticle Diffusion</u>: Building upon our earlier study,[28] we crafted trilayer-samples comprised of a thin PNC layer placed between two thick P2VP matrix layers. Upon annealing NPs diffuse into the homopolymer layers and we measure the NP tracer diffusion coefficient, D_{NP}.[28] The P2VP matrix films were prepared via spin coating; the P2VP base-layer was created by spin coating a viscous P2VP-methanol (MeOH) solutions at 1000-2000 rpm for 1 minute onto Si wafers to achieve a ~ 4 μm matrix film. To prepare the PNC mid-layers, 10 vol% SiO_2 NP or 5 vol% Al_2O_3 NP were suspended in P2VP MeOH solutions of varying concentrations and spin-coated onto SiO_2 wafers at 1000-2000 rpm for 1 min to achieve a thickness of 200 ± 60 nm. PNC layer thicknesses were measured via scanning electron microscopy (SEM), and thickness averaged over two samples. The P2VP top layers were spin-coated from varying

concentration P2VP solutions onto SiO_2 wafers (~ 4 μm). Specific solution concentrations and spin coating conditions for each layer are noted in **Table S2 and S3**. Similar to our previous report,[28] each PNC layer was transferred to a P2VP base-layer by etching the spuncoat PNC layer off the SiO_2 wafer using a 20 wt% NaOH solution, resulting in a floating PNC film that can be rinsed with DI water and stacked on top of the P2VP base-layer. The top P2VP layer was transferred to the bilayer similarly. Each trilayer specimen was annealed in a specialized custom-built oven, precisely set at 180 °C under vacuum conditions (< 50 Pa) for durations spanning from 10 minutes to 10 days. Annealing times were selected to achieve diffusion distances of ~0.5 – 3 μm.

Preparing Trilayer Samples for ToF-SIMS: To obtain the cross-sectional view, a diamond scribe was used to fracture samples along a crystallographic plane of the silicon wafer to preserve the polymer/wafer interface. Samples were cleaned with a nitrogen gas gun to remove SiO_2 dust on the surface. Carbon paint suspended in MEK was applied across the back of the wafer to reduce surface charging and improve ion yield.

ToF-SIMS: Time-of-flight secondary ion mass spectrometry is a powerful surface analysis technique that provides 3D compositional information. In ToF-SIMS, a focused beam of high-energy ions sputters molecular fragments from the material and a mass spectrometer analyzes the resulting secondary ions to determine their mass-to-charge ratio, resulting in a 2D compositional map as each layer is removed.[29] ToF-SIMS has a wide range of applications in polymer science, particularly for the analysis of surface and interface properties of polymers and polymer composites.[30–33] Our previous work produced accurate SiO_2 NP and polystyrene diffusion coefficients, and established ToF-SIMS as a powerful technique to measure both polymer and NP diffusion given the diffusing species produce ions that are distinct from the background matrix.[28]

ToF-SIMS measurements were performed using the Tescan S8252X dual-beam plasma FIB-SEM with Xe^+. Unless otherwise noted, measurements were taken with Xe^+ FIB parameters at 30 keV and 100 pA with 1024 × 1024 pixel resolution on positive ion mode for 300 (SiO_2 NPs) or 400 frames (Al_2O_3 NPs). Additional frames were collected for the Al_2O_3 NPs to improve the signal due to the lower NP loading (5 vol%) present. A 20 × 20 μm^2 field of view (FoV) was used during collection, and the ToF-SIMS images were produced using a 2 × 2 bin width, resulting in a 512 × 512-pixel image.

NP diffusion coefficients are determined by allowing NPs to travel for a set time (t = 10 min – 10 days) at a chosen temperature (T = 180°C) and measuring the corresponding NP concentration profiles using ToF-SIMS. Cross-sectioned trilayer samples were measured by scanning across the P2VP/PNC/P2VP interfaces using the Xe^+ beam, which produces the 3D ion intensity map for each mass/charge (*m/q*) value. To detect the SiO_2 and Al_2O_3 NP concentrations, we use *m/q* = 28 and 27, respectively (**Figure S1**). 1D concentration profiles were extracted from the 3D dataset by integrating along the x and z directions after tilting the data set to align the plane of the highest NP concentration within the sample to y = 0.[28] We then deconvolute the beam resolution function (Gaussian with FWHM = 0.2 μm) from the raw concentration profile to obtain the ion concentration profile. This 1D concentration profile was iteratively fit to Fick's second law for a finite source diffusing into a semi-infinite medium using

$$\varphi(y) = \frac{1}{2}\left[\mathrm{erf}\left(\frac{h-y}{\sqrt{4D_{NP}t}}\right) + \mathrm{erf}\left(\frac{h+y}{\sqrt{4D_{NP}t}}\right)\right] \qquad (6)$$

where $\varphi(y)$ is the NP concentration as a function of position y, h is the initial thickness of the PNC layer, t is time in seconds, and D_{NP} is the NP diffusion coefficient. By this process we determine D_{NP} and demonstrated in our prior work.[28]

Results and Discussion

NP Diffusion Coefficients as a Function of Molecular Weight

We measured NP diffusion into P2VP matrices of molecular weights from 14 – 1220 kDa using our ToF-SIMS method to measure NP diffusion coefficients, D_{NP}, in entangled polymer melts. We obtain diffusion coefficients after annealing for two or three annealing times to demonstrate that the NP tracer diffusion is independent of annealing time. We employ the radius of gyration (R_g) as a metric for polymer size. **Figure 1** shows representative SiO_2 (R_{NP} – 26.2 nm) and Al_2O_3 (R_{NP} = 6.5 nm) NP concentration profiles after various annealing times at 180 °C in 41 kDa P2VP (R_g = 5.5 nm) along with fits to Eqn. 6 to obtain the diffusion coefficients. In this $R_g < R_{NP}$ regime (d_T = 23.5 nm), the smaller Al_2O_3 NPs diffuse faster than the larger SiO_2 NPs and the results are consistent with $D_{core\text{-}shell}$ (Eqn 2). Specifically, $\langle D_{NP}$ (SiO_2, 26.2 nm)$\rangle = 2.8 \pm 2.0 \times 10^{-13}$ cm^2/s and $D_{core\text{-}shell}$ for this system is 3.1×10^{-13} cm^2/s and $\langle D_{NP}$ (Al_2O_3, 6.5 nm)$\rangle = 7.4 \pm 2.5 \times 10^{-13}$ cm^2/s and $D_{core\text{-}shell}$ for this system is 9.0×10^{-13} cm^2/s. Fitting the NP concentrations profiles is repeated in six other molecular weights and allows us to obtain diffusion coefficients across orders of magnitude by adjusting the annealing time. The experimental concentration profiles for all NP/P2VP systems and their respective fits are given in **Figure S2-4**, with tabulated data in **Table S4-S6**. While most of the systems studied found $D_{NP} \approx D_{core\text{-}shell}$, we also found systems having $D_{NP} > D_{core\text{-}shell}$ indicating the presence of a vehicular mechanism of NP diffusion in entangled polymer melts.

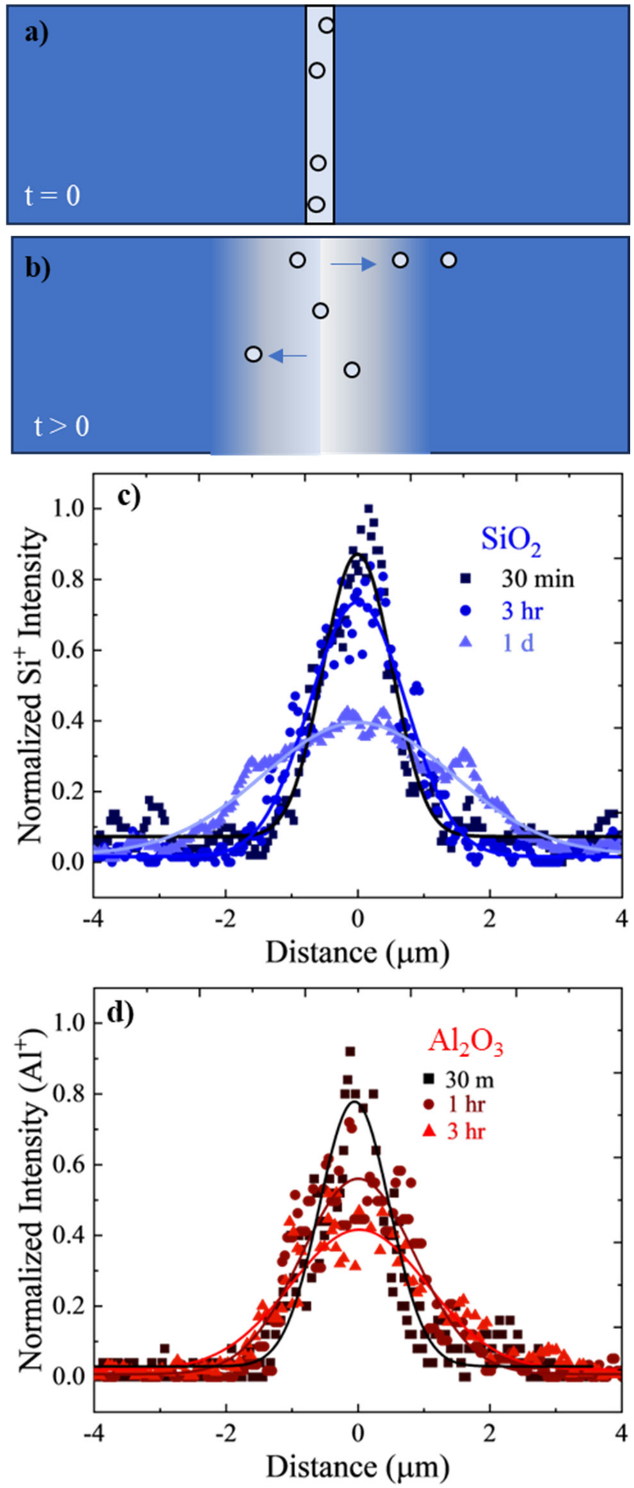

Figure 1: **a)** Initial sample state at $t = 0$, where thick P2VP layers border a thin center PNC layer. **b)** Schematic of sample after annealing for a specified time t. **c)** Concentration profiles and fits to Eqn. 6 of Si^+ signal indicating diffusion of SiO_2 NPs in 41 kDa P2VP ($R_g/R_{NP} = 0.21$) at three annealing times. **d)** Concentration profiles and fits of integrated Al^+ data indicating Al_2O_3 NP diffusion in 41 kDa P2VP ($R_g/R_{NP} = 0.85$) at three annealing times.

Core-Shell and Vehicle Diffusion Behavior

In contrast to our earlier experimental investigations, this study involves P2VP matrices spanning a wider molecular weight range of 14 – 1220 kDa, which includes unentangled to well-entangled ($M_e \approx 18$ kDa) polymer melts. To accommodate the high viscosity matrices, diffusion times were carefully controlled from 10 min – 10 days to achieve diffusion lengths commensurate with ToF-SIMS measurements. Thus, we measure D_{NP} values ranging from 7×10^{-18} to 1.3×10^{-11} cm^2/s, which is sufficient to capture both the core-shell and vehicular NP diffusion mechanism.

The larger SiO_2 NPs (R_{NP} = 26 nm) clearly exhibit core-shell model behavior across the entire molecular weight range. In **Figure 2**, the D_{NP} values from the different annealing times are normalized by $D_{core\text{-}shell}$ (Eqn. 2) and the values are on the order of 1. Similarly, the diffusion coefficients for smaller SiO_2 NPs (R_{NP} = 8.3 nm) also follow core-shell behavior even at $R_g/R_{NP} > 1$. **Figure S5** plots these D_{NP} values on a log scale wherein the data from the different annealing times are easier to distinguish. Figure 2 also includes earlier data from our group studying quantum dots in PPG where $R_g/R_{NP} < 1$ and the surface chemistry of the quantum dots was either attractive ($R_{eff} = R_{NP} + R_g$) or neutral ($R_{eff} = R_{NP}$) toward the PPG. In both cases, D_{NP} is well-described by $D_{core\text{-}shell}$.[25]

In contrast, the diffusion coefficient of the Al_2O_3 NPs (R_{NP} = 6.5 nm) deviates significantly from the core-shell mechanism of NP diffusion, Figure 2. While $D_{NP}/D_{core\text{-}shell} \approx 1$ when $R_g/R_{NP} < 1.4$, $D_{NP}/D_{core\text{-}shell}$ increases dramatically at higher R_g/R_{NP}. For example, when the P2VP matrix is M_w = 310 kg/mol and R_g/R_{NP} = 2.4, $\langle D_{NP}\rangle/D_{core\text{-}shell}$ is 17 and when the P2VP matrix is M_w = 474 kg/mol and R_g/R_{NP} = 2.9, $\langle D_{NP}\rangle/D_{core\text{-}shell}$ is 60. Consequently, we conclude that the Al_2O_3 NPs diffuse by a combination of core-shell and vehicular mechanisms. Interestingly, the Al_2O_3 NPs exhibit vehicular diffusion while similarly sized SiO_2 NPs exhibit only core-shell diffusion (see blue squares at $R_g/R_{NP} > 2$), which implies a difference in surface chemistry leads to a faster desorption time for Al_2O_3 NPs. In Figure 2b, Al_2O_3 NP behavior diverges strongly from $D_{core\text{-}shell}$ predictions and at $R_g/R_{NP} \geq 2.4$ the discrepancy between D_{NP} and $D_{core\text{-}shell}$ is ~ 10^{-14} cm^2/s, **Table S8**. Importantly, this difference ($D_{NP} - D_{core\text{-}shell}$) is nominally independent of molecular weight. Thus, we attribute the faster NP diffusion to the vehicular mechanism given by $D_{vehicle-II}$ (Eqn 4), which is independent of M_w and has a strong dependence on monomer desorption time, $\tau_{des}^{-3/4}$.

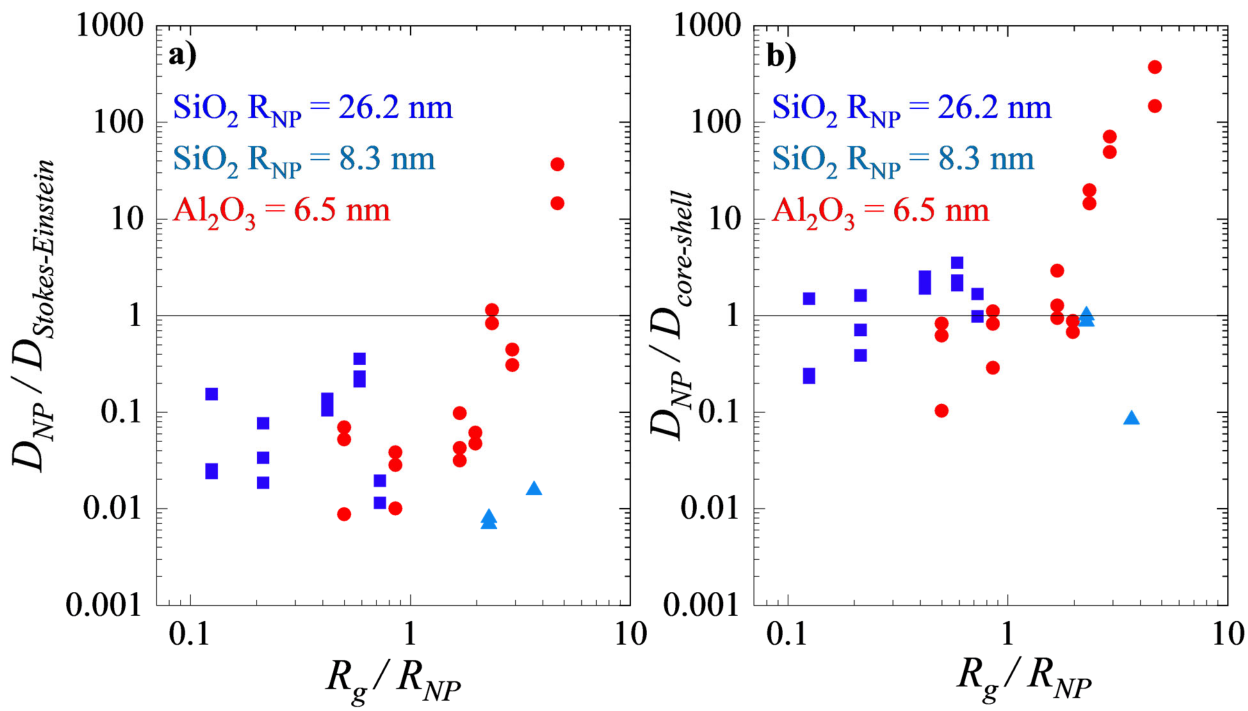

Figure 2: Nanoparticle diffusion coefficients normalized by **a)** $D_{Stokes\text{-}Einstein}$ and **b)** $D_{core\text{-}shell}$ as a function of the polymer R_g normalized by R_{NP}. Silica nanoparticles are displayed in blue squares (R_{NP} = 26.2 nm) and light blue triangles (R_{NP} = 8.3 nm). Alumina nanoparticles are displayed in red circles (R_{NP} = 6.5 nm). All annealing times are plotted.

Monomer Desorption Time of the Bound Layer

The vehicular and core-shell diffusion mechanisms both contribute to the nanoparticle diffusion coefficient (D_{NP}) and are predicated on the existence and lifetime of a bound polymer layer formed through physical adsorption. Core-shell diffusion dominates in systems where the bound layer is long-lived. In contrast, vehicular diffusion occurs in intermediately attractive systems where the rate of stochastic polymer-NP desorption is faster than that observed in core-shell behavior. An essential facet of vehicular diffusion involves understanding the monomer desorption time (τ_{des}), a topic not fully explored in nanocomposites with attractive polymer-NP interactions.[17,34] Previous studies of silica NPs in P2VP have hinted at a temperature dependence on the bound layer, revealing an effective shell radius and an exchange rate of approximately ~100 hours.[35] However, factors influencing desorption time, including polymer-NP interaction strength, molecular weight, entanglement, and NP curvature, remain largely uncharted. This knowledge gap about τ_{des} complicates our grasp of vehicular diffusion, making it challenging to pinpoint the predominant factors influencing fast diffusion. Here, we extract timescales from our prior work to interpret our NP diffusion results, refine our understanding of the vehicular mechanism, and estimate τ_{des} in these PNCs.

To isolate the effect of τ_{des}, we refine Eqn. 1 to account for both nanoparticle size and polymer molecular weight and to specify Regime II of the vehicular mechanism,

$$D_{NP,theory}(R_{NP}, \mathrm{M_w}) = D_{core-shell}(R_{NP}, \mathrm{M_w}) + Ad_T(b^2 D_0)^{\frac{1}{4}} \times \left(\frac{1}{\tau_{\mathrm{des}}}\right)^{\frac{3}{4}} \quad (7)$$

Note that Regime I of the vehicular mechanism was dismissed because the NPs in this study have surface hydroxyl groups that have favorable interactions with the nitrogen in P2VP, resulting in slower desorption times. Given $\tau_e \sim 1$ s and $D_0 = 1.0 \times 10^{-9}$ cm^2/s, we estimate $D_{\mathrm{vehicle\text{-}I}} \sim 10^{-9}$ cm^2/s, which is faster than any of our results even in the lowest M_w. This is consistent with prior results demonstrating that silica nanoparticles with hydroxyl surface groups strongly interact with P2VP to have long desorption times.[35–37] Regime III is dismissed because $D_{vehicle}$ fails to demonstrate a ~$1/N^{-1/2}$ scaling across M_w 310 – 474 kDa (Eqn. 5). The molecular weight dependence of $D_{core\text{-}shell}$ (Eqn. 2) is caused by the molecular weight dependence of R_{eff} and η_{PNC}. The effective nanoparticle radius, R_{eff}, includes a strongly polymer bound layer, $R_{eff} = R_{NP} + R_g$ and the molecular weight dependence of R_g in the melt is well known.[38] The viscosity of the PNC (η_{PNC}) is a function of the average volume fraction of the nanoparticles after dilution φ_{NP}, and polymer molecular weight

$$\eta_{PNC} = \eta_{poly}\left(1 + 2.5\varphi_{eff} + 6.2{\varphi_{eff}}^2\right) \tag{8}$$

$$\varphi_{eff} = \varphi_{NP}\left(\frac{R_{eff}}{R_{NP}}\right)^3 \tag{9}$$

We measured the melt viscosity of the P2VP polymers in this study and fit the data to obtain $\eta_{poly}(M_w)$ for Eqn 8. To capture the Regime II vehicular contribution to $D_{NP,\mathrm{theory}}$, we start with the molecular weight dependence of the shortest Rouse time (τ_0) for P2VP as previously measured by broadband dielectric spectroscopy (BDS) at $T = 413$ °K.[13] By assuming a $1/T$ dependence we adjust the measured values to temperature of interest $T = 453$ °K (180 °C), and $\tau_0 \approx 10^{-5}$ s, **Figure S6**. Then we compute all the relevant timescales by

$$\tau_e = \tau_0 * {N_e}^2 \tag{10}$$

$$\tau_{Rouse} = \tau_0 * N^2 \tag{11}$$

$$\tau_{rep} = \tau_{Rouse} * \frac{N}{N_e} \tag{12}$$

As previously mentioned, the Al_2O_3 nanoparticles appear to be in Regime II because the difference between the measured D_{NP} and $D_{core\text{-}shell}$ is independent of molecular weight. Regime II corresponds to $\tau_e < \tau_{des} < \tau_{Rouse}$, which for P2VP at 180°C indicates that τ_{des} is expected to be longer than $\tau_e \sim 1$ s and shorter than 30 – 6,000 sec corresponding to ~ 100 to 1220 kDa.

Figure 3a shows the fit of Eqn. 7 to D_{NP} for the large SiO_2 NPs as a function of molecular weight. Consistent with Figure 2, the core-shell mechanism is sufficient to describe NP diffusion of the SiO_2 NPs across all molecular weights. This implies $D_{vehicle} \sim 0$, and therefore τ_{des} (> 6000 s) is exceedingly large and consistent with a highly attractive P2VP- SiO_2 interaction. **Figure 3b** shows the experimental data for the Al_2O_3 NPs along with the fit to Eqn. 7 using $A = 1$, $d_T = 23.5$ nm, $b = 1.8$ nm, and $D_0 = 1.0 \times 10^{-9}$ cm²/s.[13] The best fit corresponds to $\tau_{des} = 50$ s, which falls within the bounds established above. To illustrate the bounds corresponding to Regime II of vehicular NP diffusion, we plot Eqn 7 using the $\tau_{des} = \tau_e$, which is independent of M_w, and $\tau_{des} = \tau_{Rouse}$, which increases with M_w. These upper and lower limits of D_{NP} for the Al_2O_3 NPs in P2VP further to confirm that this system is in Regime II at 180 °C.

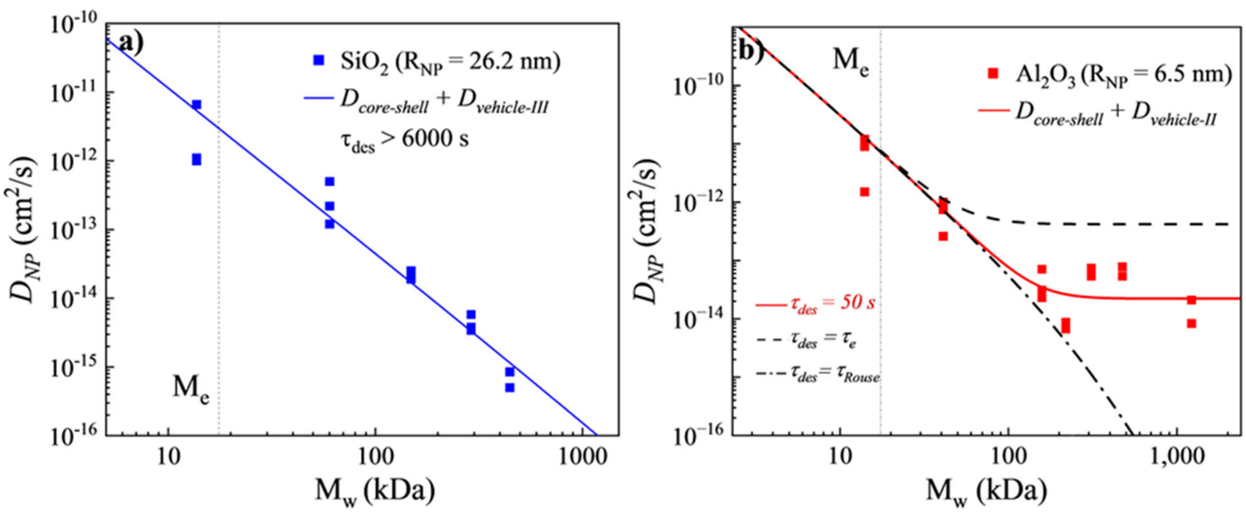

Figure 3: **a)** D_{NP} (blue points) for SiO_2 (26.2 nm) NPs in P2VP as a function of molecular weight. Solid line corresponds to D_{theory} in Eqn. 7 where $D_{vehicle} \rightarrow 0$ as $\tau_{des} >> \tau_{Rouse}$. b) D_{NP} (red points) for Al2O3 (6.5 nm) NPs in P2VP as a function of molecular weight. Red line is the best fit to Eqn 7 and corresponds to $\tau_{des} = 50$ s. Black dashed and dot-dash lines correspond to $\tau_{des} = \tau_e$ and $\tau_{des} = \tau_{Rouse}$, respectively.

These results indicate that NP diffusion coefficients can provide valuable insight into the monomer desorption times and polymer-NP interactions. Given that the core-shell behavior of small SiO_2 NPs (Figure 2) and the vehicular mechanism found in Al_2O_3 NPs of similar size, our results show that Al_2O_3 NPs exhibit weaker polymer-NP interactions. This finding is consistent with water contact angle measurements for silica (~ 80°) and alumina (~ 90°) that suggest a lower areal density of hydroxyl groups on alumina leading to weaker interactions consistent with a short τ_{des}.[39,40] Additionally, poly(vinylpyrrolidone) (PVP)preferentially adsorbs to unmodified silica particles over alumina-coated counterparts in aqueous solution, and the preadsorbed PVP transfers from the alumina-coated particles to silica particles as the system equilibrates. Adsorption isotherms further demonstrate that PVP adhesion to silica particles is stronger than to alumina-coated silica particles, which demonstrates that the silica particle surface is more polar.[41] This result is consistent with our finding that the monomeric desorption time of P2VP is longer for silica NPs than for alumina NPs. Overall, this study establishes that both the relative size of the polymer to the nanoparticle (R_g/R_{NP}) and the polymer-NP interfacial interactions dictate the transition for NP diffusion from a solely core-shell behavior mechanism to the addition of vehicular mechanisms. Further investigations could explore various methods for controlling polymer-NP interactions, including using random copolymers, as well as the effect of nanoparticle shape on diffusion.

Conclusions

We experimentally demonstrate both the core-shell and the vehicle mechanisms for nanoparticle diffusion. While large and small silica NPs demonstrate the core-shell mechanism (Eqn. 2) due to highly attractive polymer-NP interactions and long monomer desorption times, τ_{des}, small alumina nanoparticles display a crossover from core-shell to vehicular NP diffusion. For the Al_2O_3 NPs, D_{NP} exhibits a plateau as M_w increases and $R_g > R_{NP}$, and this molecular weight independent behavior is consistent with Regime II of the vehicular mechanism. At high M_w, the

Al_2O_3 NP diffusion coefficients are one or two orders of magnitude faster than predicted by the core-shell model alone. Fitting the data reveals a τ_{des} of ~ 50 s that is independent of M_w and indicates a weaker polymer-NP interaction in P2VP/Al_2O_3 than in P2VP/SiO_2 nanocomposites. We have demonstrated that by measuring nanoparticle diffusion coefficients in polymer melts, one can determine the polymer-NP interaction strengths, which has previously been difficult to ascertain. This study provides a pathway to measure monomer desorption times (τ_{des}) for a variety of PNC systems to explore the role of temperature, NP size, NP surface functionality, and polymer composition to understand the lifetime of the polymer bound layer on nanoparticles. We found that the core-shell and vehicle diffusion modes apply broadly to entangled melts with attractive polymer-NP interactions.

Supporting Information

Table S1: Molecular weight characterization of P2VP and calculated R_g.

Table S2: Spincoating conditions to create P2VP films.

Table S3: Spincoating conditions to create polymer nanocomposite films.

Figure S1: ToF SIMS mass spectra distinguished m/q = 27 (Al^+) and m/q = 28 (Si^+) peaks.

Figure S2: Normalized concentration profiles from ToF SIM for SiO_2 nanoparticles (R_{NP} = 26.2 nm) diffusing into P2VP (M_w = 14.0 - 474 kDa).

Figure S3: Normalized concentration profiles from ToF SIM for Al_2O_3 nanoparticles (R_{NP} = 6.5 nm) diffusing into P2VP (M_w = 14.0 - 1220 kDa).

Figure S4: Normalized concentration profiles from ToF SIM for SiO_2 nanoparticles (R_{NP} = 8.3 nm) diffusing into P2VP (M_w = 474 and 1220 kDa).

Table S4: Measured diffusion coefficients for large SiO_2 (R_{NP} = 26.2 nm) in P2VP (14.0 – 474 kDa).

Table S5: Measured diffusion coefficients for small Al_2O_3 (R_{NP} = 6.5 nm) in P2VP (14.0 – 1220 kDa).

Table S6: Measured diffusion coefficients for small SiO_2 (R_{NP} = 8.3 nm) in P2VP (474 and 1220 kDa).

Table S7: Nanoparticle diffusion coefficients from the core-shell model ($D_{core\text{-}shell}$) at T = 180 °C as a function of molecular weight.

Figure S5: $D_{NP}/D_{core\text{-}shell}$ versus R_g/R_{NP} showing data from all annealing times.

Table S8: Evidence for Regime II vehicular diffusion.

Figure S6: Shortest Rouse time (τ_0) for P2VP measured at 140 **°C** and scaled to 180 **°C** .

Acknowledgments

We acknowledge funding from NSF CBET 2034122. We thank Dr. Jamie Ford at the Singh Center for Nanotechnology at the University of Pennsylvania for his expertise regarding ToF-SIMS, supported by NSF-MRSEC-DMR-2309043. We thank Roshni John Chethalen at the University of Massachusetts Amherst for providing GPC analysis. We thank Ravisara Wattana at the University of Pennsylvania for providing viscosity characterization of P2VP. We thank Dr. Eric Bailey and Dr. Will Drayer for insightful discussions.

Competing interests

The authors declare no competing interests.

References:

(1) Kumar, S. K.; Benicewicz, B. C.; Vaia, R. A.; Winey, K. I. 50th Anniversary Perspective: Are Polymer Nanocomposites Practical for Applications? *Macromolecules* **2017**, *50*, 714–731.

(2) Méar, F.; Coillot, D.; Podor, R.; Montagne, L. Self-Healing Nanocomposites: Role and Activation of Inorganic Moieties and Hybrid Nanophases. In *{Self-Healing} at the Nanoscale*; CRC Press, 2011; pp 188–223.

(3) Mallakpour, S.; Naghdi, M. {Polymer/SiO2} Nanocomposites: Production and Applications. *Prog. Mater. Sci.* **2018**, *97*, 409–447.

(4) Thakur, V. K.; Kessler, M. R. Self-Healing Polymer Nanocomposite Materials: A Review. *Polymer (Guildf).* **2015**, *69*, 369–383.

(5) Young, W. W.; Katsumata, R. Intermediate Polymer Relaxation Explains the Anomalous Rheology of Nanocomposites with Ultrasmall Attractive POSS Nanoparticles. *ACS Polym. Au* **2023**, *3*, 466–474.

(6) Merkel, T. C.; Freeman, B. D.; Spontak, R. J.; He, Z.; Pinnau, I.; Meakin, P.; Hill, A. J. Ultrapermeable, Reverse-Selective Nanocomposite Membranes. *Science (80-.).* **2002**, *296*, 519–522.

(7) Yin, J.; Deng, B. Polymer-Matrix Nanocomposite Membranes for Water Treatment. *J. Memb. Sci.* **2015**, *479*, 256–275.

(8) Cheng, S.; Xie, S.-J.; Carrillo, J.-M. Y.; Carroll, B.; Martin, H.; Cao, P.-F.; Dadmun, M. D.; Sumpter, B. G.; Novikov, V. N.; Schweizer, K. S.; Sokolov, A. P. Big Effect of Small Nanoparticles: A Shift in Paradigm for Polymer Nanocomposites. *ACS Nano* **2017**, *11*, 752–759.

(9) Balazs, A. C.; Emrick, T.; Russell, T. P. Nanoparticle Polymer Composites: Where Two Small Worlds Meet. *Science (80-.).* **2006**, *314*, 1107–1110.

(10) Lin, C.-C.; Parrish, E.; Composto, R. J. Macromolecule and Particle Dynamics in Confined Media. *Macromolecules* **2016**, *49*, 5755–5772.

(11) Cheng, S.; Holt, A. P.; Wang, H.; Fan, F.; Bocharova, V.; Martin, H.; Etampawala, T.; White, B. T.; Saito, T.; Kang, N.-G.; Dadmun, M. D.; Mays, J. W.; Sokolov, A. P. Unexpected Molecular Weight Effect in Polymer Nanocomposites. *Phys. Rev. Lett.* **2016**, *116*, 038302-1–4.

(12) Papakonstantopoulos, G. J.; Yoshimoto, K.; Doxastakis, M.; Nealey, P. F.; De Pablo, J. J. Local Mechanical Properties of Polymeric Nanocomposites. *Phys. Rev. E - Stat. Nonlinear, Soft Matter Phys.* **2005**, *72*, 031801-031801–031806.

(13) Bailey, E. J.; Griffin, P. J.; Composto, R. J.; Winey, K. I. Multiscale Dynamics of Small, Attractive Nanoparticles and Entangled Polymers in Polymer Nanocomposites. *Macromolecules* **2019**, *52*, 2181–2188.

(14) Griffin, P. J.; Bocharova, V.; Middleton, L. R.; Composto, R. J.; Clarke, N.; Schweizer, K. S.; Winey, K. I. Influence of the Bound Polymer Layer on Nanoparticle Diffusion in Polymer Melts. *ACS Macro Lett.* **2016**, *5*, 1141–1145.

(15) Cheng, S.; Carroll, B.; Bocharova, V.; Carrillo, J.-M.; Sumpter, B. G.; Sokolov, A. P.; Carrillo, J.-M. Y. Perspective: Outstanding Theoretical Questions in Polymer-Nanoparticle Hybrids. *J. Chem. Phys.* **2017**, *146*, 203201.

(16) Yamamoto, U.; Carrillo, J.-M. Y.; Bocharova, V.; Sokolov, A. P.; Sumpter, B. G.; Schweizer, K. S. Theory and Simulation of Attractive Nanoparticle Transport in Polymer

Melts. *Macromolecules* **2018**, *51*, 2258–2267.
(17) Carroll, B.; Bocharova, V.; Carrillo, J.-M. Y.; Kisliuk, A.; Cheng, S.; Yamamoto, U.; Schweizer, K. S.; Sumpter, B. G.; Sokolov, A. P. Diffusion of Sticky Nanoparticles in a Polymer Melt: Crossover from Suppressed to Enhanced Transport. *Macromolecules* **2018**, *51*, 2268–2275.
(18) Tuteja, A.; Mackay, M. E.; Narayanan, S.; Asokan, S.; Wong, M. S. Breakdown of the Continuum Stokes-Einstein Relation for Nanoparticle Diffusion. *Nano Lett.* **2007**, *7*, 1276–1281.
(19) Lin, C.-C.; Gam, S.; Meth, J. S.; Clarke, N.; Winey, K. I.; Composto, R. J. Do Attractive Polymer−Nanoparticle Interactions Retard Polymer Diffusion in Nanocomposites? **2013**, *46*, 42.
(20) Liu, J.; Cao, D.; Zhang, L. Molecular Dynamics Study on Nanoparticle Diffusion in Polymer Melts: A Test of the Stokes-Einstein Law. *J. Phys. Chem. C* **2008**, *112*, 6653–6661.
(21) Grabowski, C. A.; Mukhopadhyay, A. Size Effect of Nanoparticle Diffusion in a Polymer Melt. *Macromolecules* **2014**, *47*, 7238–7242.
(22) Cai, L. H.; Panyukov, S.; Rubinstein, M. Hopping Diffusion of Nanoparticles in Polymer Matrices. *Macromolecules* **2015**, *48*, 847–862.
(23) Cai, L.-H.; Panyukov, S.; Rubinstein, M. Mobility of Nonsticky Nanoparticles in Polymer Liquids. *Macromolecules* **2011**, *44*, 7853–7863.
(24) Cole, D. H.; Shull, K. R.; Rehn, L. E.; Baldo, P. M. RBS Analysis of the Diffusion of Nano-Size Spheres in a Polymer Matrix. *Nucl. Instruments Methods Phys. Res. Sect. B Beam Interact. with Mater. Atoms* **1998**, *136–138*, 283–289.
(25) Park, J.; Bailey, E. J.; Composto, R. J.; Winey, K. I. Single-Particle Tracking of Nonsticky and Sticky Nanoparticles in Polymer Melts. *Macromolecules* **2020**, *53*, 3933–3939.
(26) Mendez, N. F.; Dhara, D.; Zhang, Q.; Narayanan, S.; Schadler, L. S.; Müller, A. J.; Kumar, S. K. Nanoparticle Diffusion in Miscible Polymer Nanocomposite Melts. *Macromolecules* **2023**, *56*, 4658–4668.
(27) Kwon, N. K.; Park, C. S.; Lee, C. H.; Kim, Y. S.; Zukoski, C. F.; Kim, S. Y. Tunable Nanoparticle Stability in Concentrated Polymer Solutions On the Basis of the Temperature Dependent Solvent Quality. *Macromolecules* **2016**, *20*, 25.
(28) Wang, K.; Composto, R. J.; Winey, K. I. ToF-SIMS Depth Profiling to Measure Nanoparticle and Polymer Diffusion in Polymer Melts. *Macromolecules* **2023**.
(29) Spool, A. M. *The Practice of TOF-SIMS: Time of Flight Secondary Ion Mass Spectrometry - Alan M. Spool - Google Books*; Momentum Press, 2016.
(30) Mei, H.; Laws, T. S.; Terlier, T.; Verduzco, R.; Stein, G. E. Characterization of Polymeric Surfaces and Interfaces Using Time-of-Flight Secondary Ion Mass Spectrometry. *Journal of Polymer Science*. John Wiley and Sons Inc April 1, 2021, pp 1174–1198.
(31) Prasad, A.; Salim, N. V; Mozetič, M.; Kailas, L.; Thomas, S. Time-of-flight Secondary Ion Mass Spectrometric Analysis of Polymer Surfaces: A Review. *J. Appl. Polym. Sci.* **2022**, 52286.
(32) Karar, N.; Gupta, T. K. Study of Polymers and Their Blends Using TOF-SIMS Ion Imaging. *Vacuum* **2015**, *111*, 119–123.
(33) Chan, C. M.; Weng, L. T. Surface Characterization of Polymer Blends by XPS and ToF-SIMS. *Materials (Basel).* **2016**, *9*.
(34) Ge, T. Scaling Perspective on Dynamics of Nanoparticles in Polymers: Length- and Time-

Scale Dependent Nanoparticle-Polymer Coupling. *Macromolecules* **2023**, *56*, 3809–3837.
(35) Jimenez, A. M.; Zhao, D.; Misquitta, K.; Jestin, J.; Kumar, S. K. Exchange Lifetimes of the Bound Polymer Layer on Silica Nanoparticles. *ACS Macro Lett.* **2019**, *8*, 166–171.
(36) Bailey, E. J.; Griffin, P. J.; Composto, R. J.; Winey, K. I. Characterizing the Areal Density and Desorption Kinetics of Physically Adsorbed Polymer in Polymer Nanocomposite Melts. *Macromolecules* **2020**, *53*, 2744–2753.
(37) Harton, S. E.; Kumar, S. K.; Yang, H.; Koga, T.; Hicks, K.; Lee, H.; Mijovic, J.; Liu, M.; Vallery, R. S.; Gidley, D. W. Immobilized Polymer Layers on Spherical Nanoparticles. *Macromolecules* **2010**, *43*, 3415–3421.
(38) Rubinstein, M.; Colby, R. H. *Polymer Physics*; Oxford University Press, 2003.
(39) Jin, J.; Wang, X.; Wick, C. D.; Dang, L. X.; Miller, J. D. Silica Surface States and Their Wetting Characteristics. *https://doi.org/10.1680/jsuin.19.00053* **2020**, *8*, 145–157.
(40) Watcharenwong, A.; Saijaioup, N.; Bailuang, Y.; Kajitvichyanukul, P. Morphology and Wettability of Nanoporous Aluminium Oxide Film Prepared by Anodization. *Key Eng. Mater.* **2017**, *737*, 174–178.
(41) Cooper, C. L.; Cosgrove, T.; Van Duijneveldt, J. S.; Murray, M.; Prescott, S. W. Colloidal Particles in Competition for Stabilizer: A Solvent Relaxation NMR Study of Polymer Adsorption and Desorption. *Langmuir* **2012**, *28*, 16588–16595.

Supporting Information

Vehicular and Core-Shell Nanoparticle Diffusion in Attractive Entangled Polymer Melts

Kaitlin Wang[1] and **Karen I. Winey**[1,2,*]

[1] Department of Materials Science and Engineering, University of Pennsylvania, Philadelphia, PA 19104, United States of America

[2] Department of Chemical and Biomolecular Engineering, University of Pennsylvania, Philadelphia, PA 19104, United States of America

***Corresponding author:** Karen I. Winey, winey@seas.upenn.edu,
Address: Laboratory for Research on the Structure of Matter, 3231 Walnut St, Philadelphia, PA 19104

List of Content

Table S1: Molecular weight characterization of poly(2-vinylpyridine) and calculated R_g. All samples were measured with tetrahydrofuran as the carrier solvent and normalized using a polystyrene standard. The radius of gyration was calculated using Rubinstein and Colby.[1]

M_w (kg/mol)	M_n (kg/mol)	PDI	Calculated R_g (nm)
14.0	13.7	1.04	3.2
41.0	40.8	1.01	5.5
158	149	1.06	10.9
219	197	1.11	12.8
310	290	1.07	15.3
474	446	1.06	18.8
1,220*	1100*	1.11	30.2

*Indicates values provided by the supplier.

Table S2: Spincoating conditions to create poly(2-vinylpyridine) films. Parameters include weight-averaged molecular weights, solution concentrations, spincoating speeds, and spin times to create the ~4 µm thick P2VP matrix films.

M_w (kg/mol)	Solution Concentration (g/L)	Spin Speed (rpm)	Spin time (sec)
14.0	450	1000	120
41.0	300	1000	120
158	250	1500	90
219	180	1500	60
310	170	2000	60
474	150	2000	60
1,220	50	1500	60

Table S3: Spincoating conditions to create polymer nanocomposite films. Parameters include weight-averaged molecular weights, solution concentrations, spincoating speeds, and spin times to create thin PNC center layers (200 ± 60 nm).

M_w (kg/mol)	Solution Concentration (g/L)	Spin Speed (rpm)	Spin time (sec)
14.0	70	1500	60
41.0	60	2000	60
158	50	2000	60
219	40	2000	60
310	35	2000	60
474	30	2000	60
1,220	20	2000	60

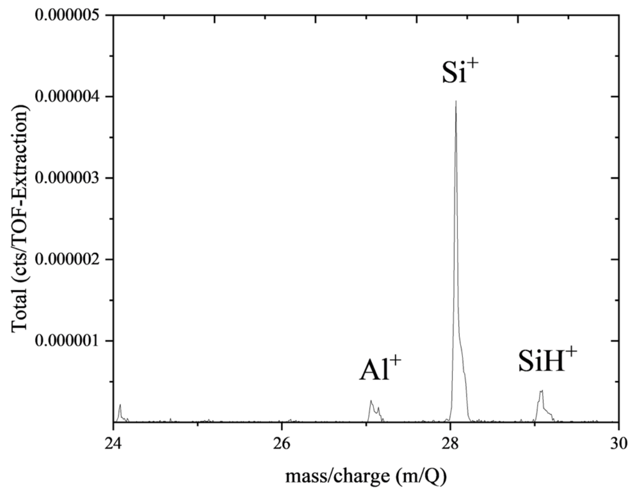

Figure S1: Mass spectra from ToF SIMS displaying distinct m/q = 27 (Al^+) and m/q = 28 (Si^+) peaks. This mass spectra demonstrates the ability to use ToF SIMS to distinguish silica and alumina nanoparticles. Sample is 158 kDa P2VP sample with 5 vol% Al_2O_3 NPs and 5 vol% SiO_2 NPs. ToF SIMS was collected at 100 pA and 30 kV conditions for 400 frames. In ToF SIMS relative peak intensities do not quantitatively indicate sample composition.

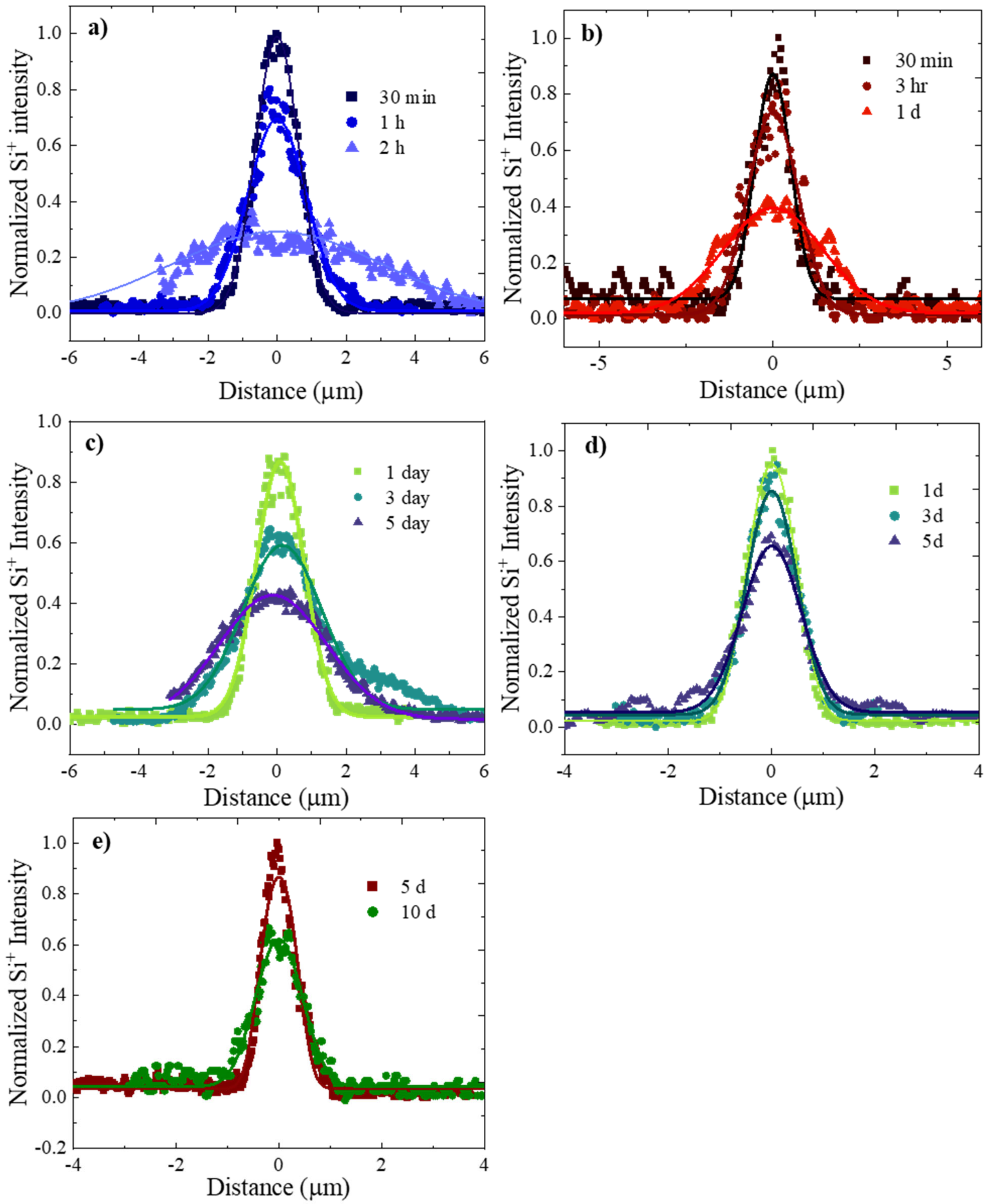

Figure S2: Normalized concentration profiles from ToF SIM for SiO_2 nanoparticles (R_{NP} = 26.2 nm) diffusing into P2VP. (**a**) 14.0 kDa, (**b**) 41.0 kDa, (**c**) 158 kDa, (**d**) 310 kDa, and (**e**) 474 kDa. Lines correspond to Fick's 2nd law and the D_{NP} and R^2 values are tabulated in **Table S4**.

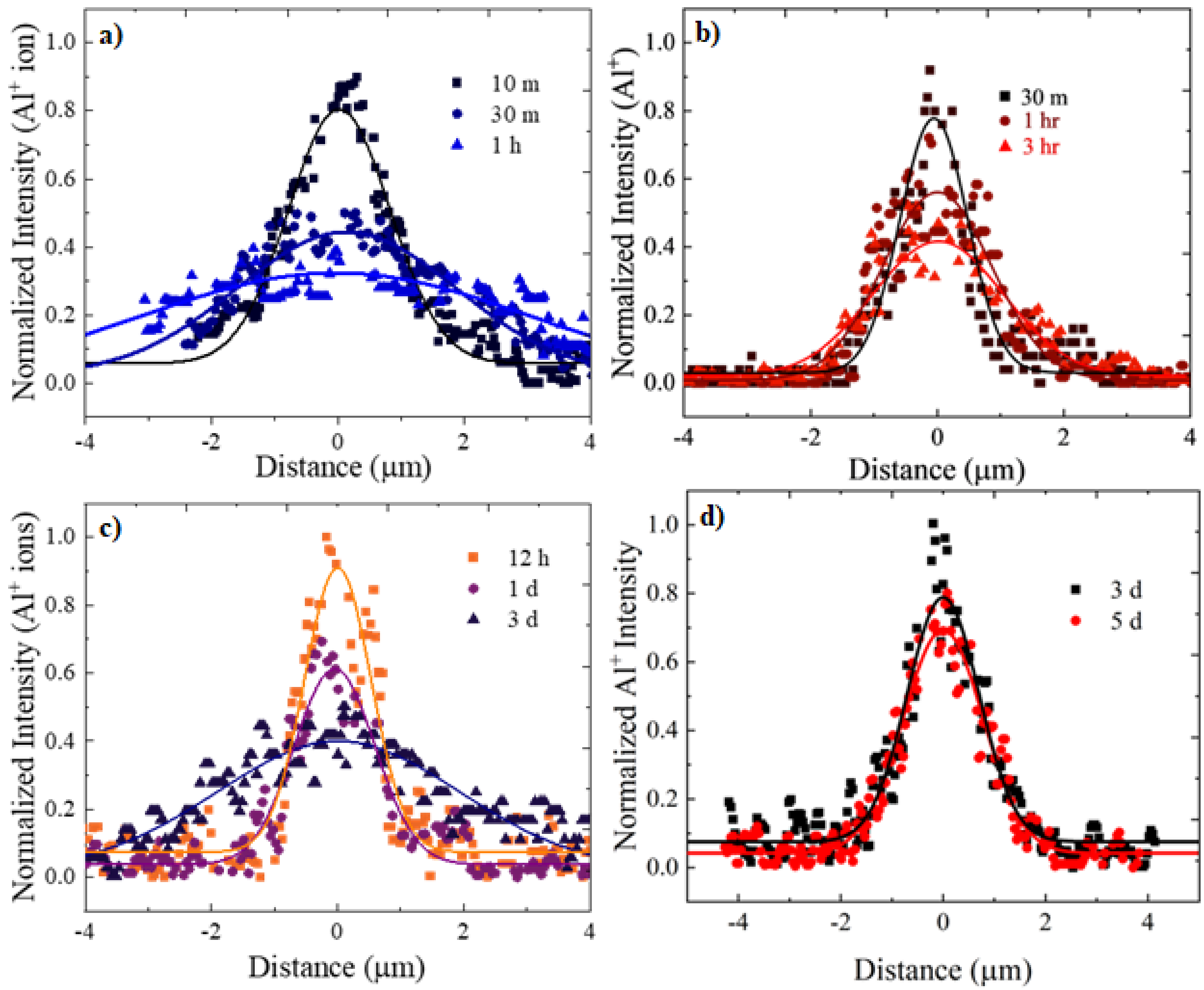

Figure continues on the next page. Figure caption on next page.

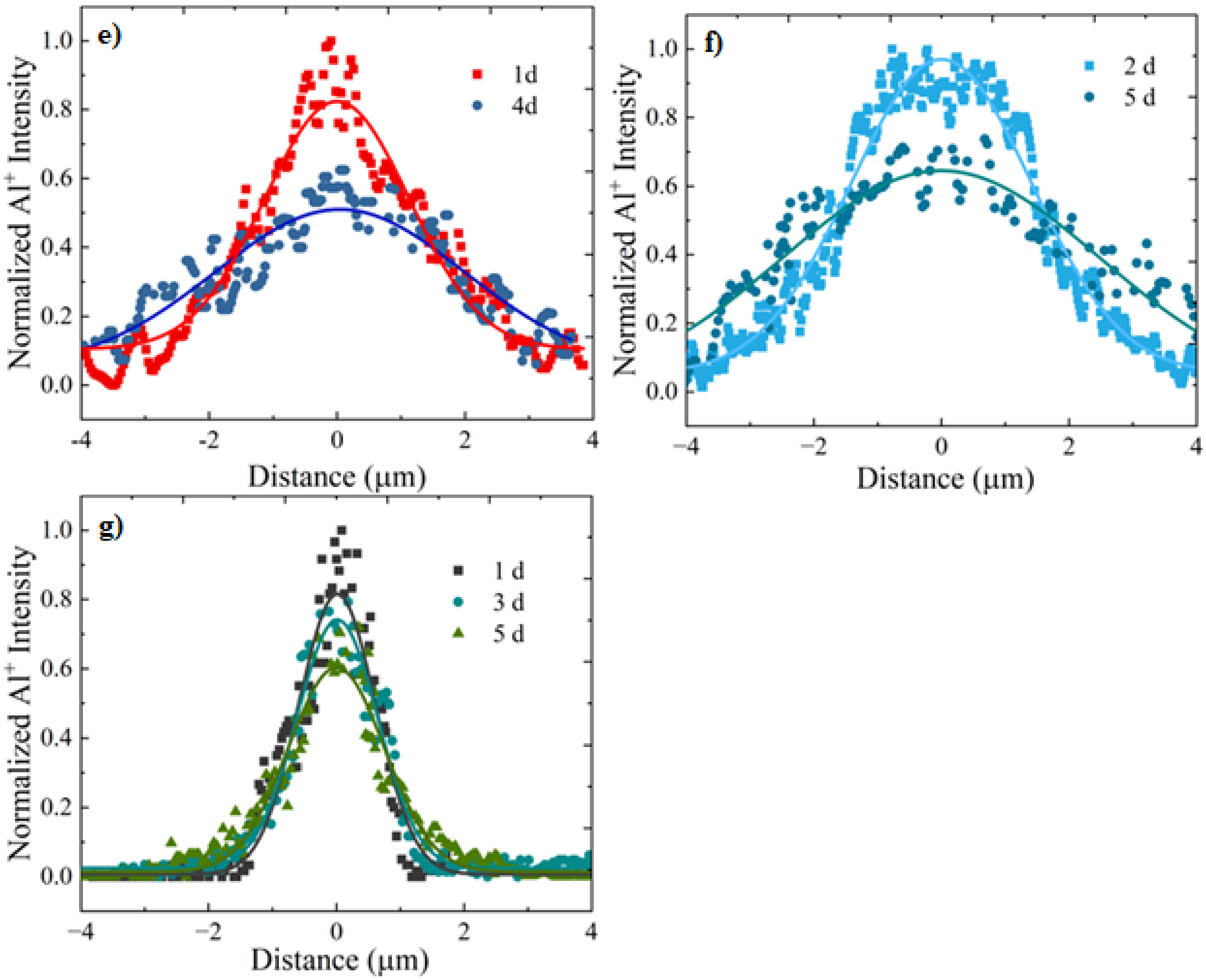

Figure S3: Normalized concentration profiles from ToF SIM for Al_2O_3 nanoparticles (R_{NP} = 6.5 nm) diffusing into P2VP (M_w = 14.0 - 1220 kDa). (**a**) 14.0 kDa, (**b**) 41.0 kDa, (**c**) 158 kDa, (**d**) 219 kDa **e)** 310 kDa, (**f**) 474 kDa, (**g**) 1220 kDa. Lines correspond to Fick's 2nd law and the D_{NP} and R^2 values are tabulated in **Table S5**.

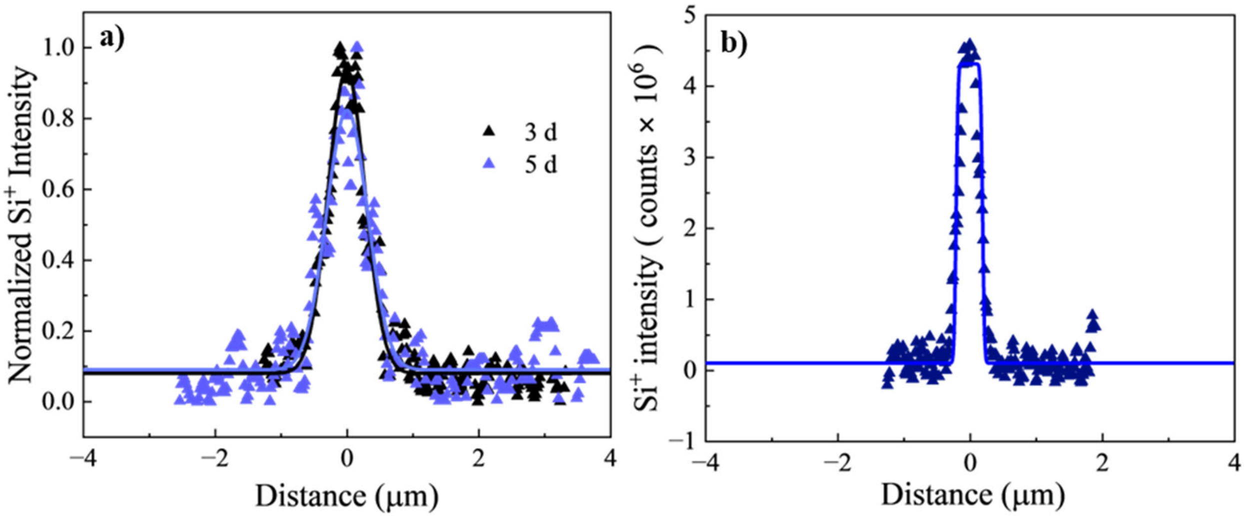

Figure S4: Normalized concentration profiles from ToF SIM for SiO_2 nanoparticles (R_{NP} = 8.3 nm) diffusing into P2VP (M_w = 474 and 1220 kDa). (**a**) 474 kDa and (b) 1220 kDa. Lines correspond to Fick's 2nd law and the D_{NP} and R^2 values are tabulated in **Table S6**.

Table S4: Measured diffusion coefficients for large SiO_2 (R_{NP} = 26.2 nm) in P2VP (14.0 – 474 kDa). Annealing times range from 30 min to 10 days.

	Sample 1		Sample 2		Sample 3		Average ± STD
M_w (kDa)	**t_1**	**D_{NP} (cm²/s) R^2**	**t_2**	**D_{NP} (cm²/s) R^2**	**t_3**	**D_{NP} (cm²/s) R^2**	**D_{NP} (cm²/s)**
14.0	30 m	1.1×10^{-12} 0.988	1 h	1.0×10^{-12} 0.968	2 h	6.2×10^{-12} 0.831	**$2.8 \pm 3.0 \times 10^{-12}$**
41.0	30 m	5.0×10^{-13} 0.932	3 h	2.2×10^{-13} 0.958	1 d	1.2×10^{-13} 0.942	**$2.8 \pm 2.0 \times 10^{-13}$**
158	1 d	2.2×10^{-14} 0.992	3 d	1.9×10^{-14} 0.990	5 d	2.5×10^{-14} 0.993	**$2.2 \pm 0.3 \times 10^{-14}$**
310	1 d	5.7×10^{-15} 0.991	3 d	3.4×10^{-15} 0.986	5 d	3.8×10^{-15} 0.972	**$4.3 \pm 1.2 \times 10^{-15}$**
474	5 d	5.0×10^{-16} 0.945	10 d	8.5×10^{-16} 0.952			**$6.8 \pm 2.5 \times 10^{-16}$**

Table S5: Measured diffusion coefficients for small Al_2O_3 (R_{NP} = 6.5 nm) in P2VP (14.0 – 1220 kDa). Annealing times range from 10 min to 5 days.

	Sample 1		Sample 2		Sample 3		Average ± STD
M_w (kDa)	**t_1**	**D_{NP} (cm²/s) R^2**	**t_2**	**D_{NP} (cm²/s) R^2**	**t_3**	**D_{NP} (cm²/s) R^2**	**D_{NP} (cm²/s)**
14.0	10 m	5.3×10^{-12} 0.956	30 m	9.0×10^{-12} 0.902	1 h	1.3×10^{-11} 0.867	**$9.1 \pm 3.8 \times 10^{-12}$**
41.0	30 m	7.4×10^{-13} 0.852	1 h	1.0×10^{-12} 0.910	3 h	4.9×10^{-13} 0.900	**$7.4 \pm 2.5 \times 10^{-13}$**
158	12 h	3.3×10^{-14} 0.851	1 d	2.6×10^{-14} 0.883	3 d	7.1×10^{-14} 0.894	**$4.3 \pm 2.4 \times 10^{-14}$**
219	3 d	8.7×10^{-15} 0.917	5 d	6.7×10^{-15} 0.944			**$7.7 \pm 1.5 \times 10^{-15}$**
310	1 d	7.4×10^{-14} 0.934	4 d	5.4×10^{-14} 0.841			**$6.4 \pm 1.4 \times 10^{-14}$**
474	2 d	5.4×10^{-14} 0.967	5 d	7.8×10^{-14} 0.881			**$6.6 \pm 1.7 \times 10^{-14}$**
1,220	1 d	2.1×10^{-14} 0.920	3 d	8.3×10^{-15} 0.939	5 d	8.3×10^{-15} 0.945	**$1.3 \pm 0.73 \times 10^{-14}$**

Table S6: Measured diffusion coefficients for small SiO_2 (R_{NP} = 8.3 nm) in P2VP (474 and 1220 kDa). Annealing times range from 3 to 5 days.

		Sample 1		**Sample 2**
M_w (kDa)	**t_1**	**D_{NP} (cm^2/s)** **R^2**	**t_2**	**D_{NP} (cm^2/s)** **R^2**
474	3 d	1.2×10^{-15} 0.958	5 d	9.5×10^{-16} 0.881
1,220	5 d	6.9×10^{-18} 0.976		

Table S7: **Nanoparticle diffusion coefficients from the core-shell model ($D_{core\text{-}shell}$) at T = 180 °C as a function of molecular weight.** Details of the calculations are below.

M_w (kDa)	R_g (nm)	$D_{core\text{-}shell}$ (cm^2/s) Al_2O_3 (R_{NP} = 6.5 nm)	$D_{core\text{-}shell}$ (cm^2/s) SiO_2 (R_{NP} = 8.3 nm)	$D_{core\text{-}shell}$ (cm^2/s) SiO_2 (R_{NP} = 26.2 nm)
14.0	3.2	1.4×10^{-11}		4.4×10^{-12}
41.0	5.5	9.0×10^{-13}		3.1×10^{-13}
158	10.9	2.4×10^{-14}		9.9×10^{-15}
219	12.8	9.9×10^{-15}		
310	15.3	3.7×10^{-15}		1.6×10^{-15}
474	18.8	1.1×10^{-15}	1.1×10^{-15}	5.1×10^{-16}
1,220	30.2	5.6×10^{-17}	8.1×10^{-17}	

In the core-shell model[2] the nanoparticle diffusion coefficient ($D_{core\text{-}shell}$) follows Stokes-Einstein behavior

$$D_{core-shell} = \frac{k_B T}{6\pi \eta_{PNC} R_{eff}} \quad \text{(S1)}$$

where k_B is the Boltzmann constant, T is the annealing temperature in Kelvin, η_{PNC} is the viscosity of the polymer nanocomposite in Pa·s, and R_{eff} is the effective radius of the particle that includes a strongly polymer bound layer, $R_{eff} = R_{NP} + R_g$.

The viscosity of the PNC is a function of the polymer molecular weight and the volume fraction of the nanoparticles. In the core-shell model, strongly bound polymers increase the effective size of the nanoparticles that also increasing the effective volume fraction of nanoparticles, as given by

$$\varphi_{eff} = \varphi_{NP} \left(\frac{R_{eff}}{R_{NP}}\right)^3 \quad \text{(S2)}$$

As the NPs diffuse from the PNC mid-layer into the P2VP matrix layers, φ_0, the initial volume fraction, overestimates φ_{NP}, the approximate diluted volume fraction in the annealed matrix. Here, from the unannealed film concentration of $\varphi_{0\text{-}SiO2} = 0.1$, we estimate the matrix $\varphi_{NP\text{-}SiO2} = 0.0250$ to account for the NP dilution during the experiment. Likewise, for our Al_2O_3 samples, where the unannealed $\varphi_{0\text{-}Al2O3} = 0.05$, we estimate the matrix $\varphi_{NP\text{-}Al2O3} = 0.01$ after dilution. Following work by Griffin *et al.,*[2] we account compute the PNC viscosity using.

$$\eta_{PNC} = \eta_{poly}\left(1 + 2.5\varphi_{eff} + 6.2{\varphi_{eff}}^2\right) \quad \text{(S3)}$$

To incorporate the effect of molecular weight, we need to modify the expressions for R_g and η_{poly}.

The molecular weight dependence of R_g is well-established. Rubinstein and Colby[1] by

$$R_g^2 = C_\infty n l^2 \tag{S4}$$

where l is the bond length, n is the number of backbone bonds, and C_∞ is the characteristic ratio. For P2VP, C-C backbone bond length l = 1.54 Å, C_∞= 10,[3] and $n = 2*M_w/M_{2VP\ monomer}$. Thus, the molecular weight dependence of the of R_g for P2VP is

$$R_g^2 = \frac{C_\infty n l^2}{6} = \frac{C_\infty \frac{M_W}{M_{2VP}} l^2}{3} \tag{S5}$$

$$R_g(\mathrm{M_w}) = l\left(\frac{C_\infty \frac{M_W}{M_{2VP}}}{3}\right)^{1/2} \tag{S6}$$

For Table S7, Eqn S6 was substituted into $R_{eff} = R_{NP} + R_g$ to reflect the molecular weight dependence of R_{eff} in Eqn S1

The molecular weight dependence of η_{poly} at 180 °C is provided from previous experimental measurements done by Griffin et al.[2] (black triangles) and new results from this study (black squares).

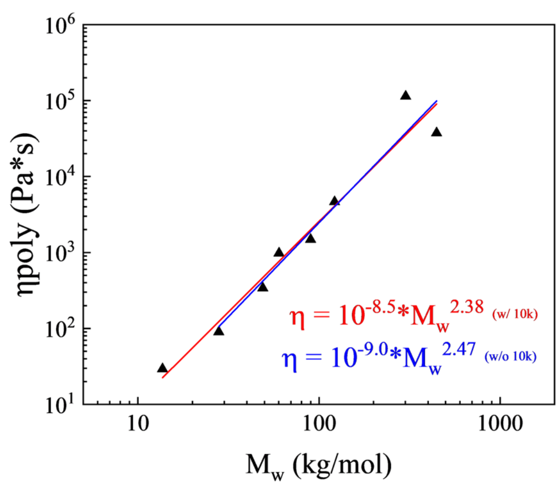

The figure includes two fits to this experimental data both with and without the lowest molecular weight P2VP sample. Although the entanglement molecular weight of P2VP is 18 kDa, the quality of the fit to the data is comparable. Thus, for Table S7, Eqn S3 uses

$$\eta_{P2VP} = 10^{-8.5} * M_w^{2.38} \tag{S7}$$

to capture the molecular weight dependence of η_{poly}.

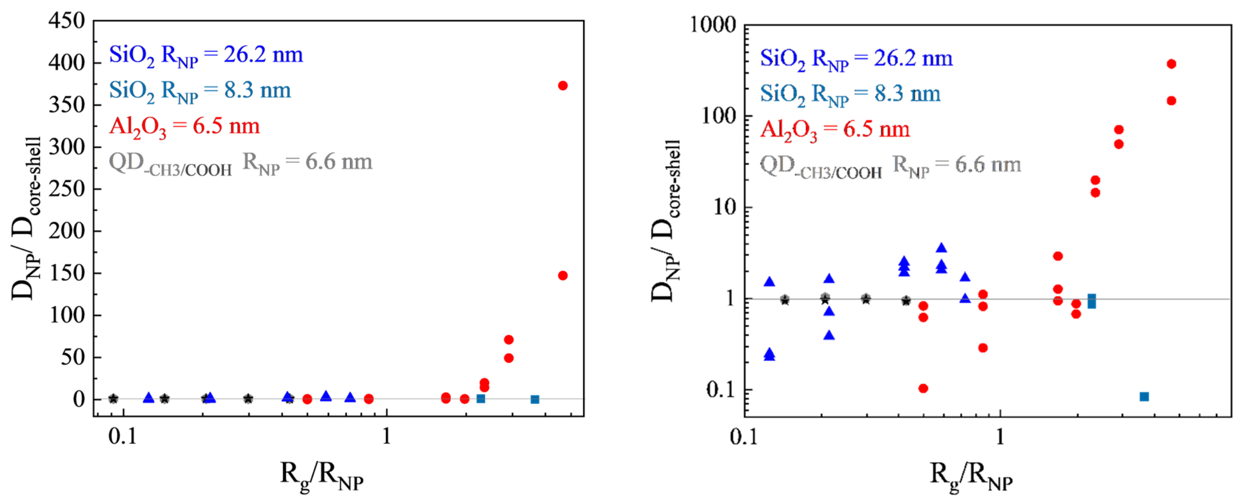

Figure S5: $D_{NP}/D_{core\text{-}shell}$ versus R_g/R_{NP} showing data from all annealing times. Silica nanoparticles are displayed in blue triangles (R_{NP} = 26.2 nm) and light blue squares (R_{NP} = 8.3 nm). Alumina nanoparticles are displayed in red circles (R_{NP} = 6.5 nm). Specific annealing times are provided in Tables S4-6. Additional data from single particle tracking experiments of methyl-capped (black stars) or carboxyl-capped (gray circles) quantum dot nanoparticles (R_{NP} = 6.6 nm) in poly(propylene glycol) (M_w = 0.425 – 8 kDa; R_g = 0.6 – 2.8 nm).[4]

Table S8: Evidence for Regime II vehicular diffusion. The difference between the average D_{NP} and $D_{core\text{-}shell}$ for Al_2O_3 NPs (R_{NP} = 6.5 nm) as a function of molecular weight. When $R_g/R_{NP} \geq 2.4$ (blue highlight), the difference becomes independent of molecular weight.

M_w (kDa)	R_g/R_{NP}	$\langle D_{NP}\rangle / D_{core\text{-}shell}$	$\langle D_{NP}\rangle - D_{core\text{-}shell}$
14.0	0.54	0.65	-5.3×10^{-12}
41.0	0.84	0.82	-1.6×10^{-13}
158	1.7	1.8	1.9×10^{-14}
219	2.0	0.78	-2.2×10^{-15}
310	2.4	17.2	6.0×10^{-14}
474	2.9	60.0	6.5×10^{-14}
1,220	4.6	232	1.3×10^{-14}

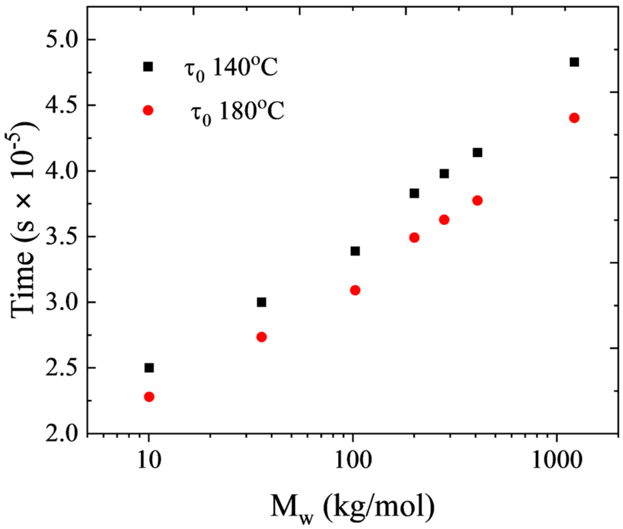

Figure S6: Shortest Rouse time (τ_0) for P2VP measured at 140 °C and scaled to 180 °C. The τ_0 values were measured at 140 °C (black) using dielectric relaxation spectroscopy.[5] Data scaled to 180 °C (red) by assuming $\tau_0 \sim 1/T$ (Kelvin).

References:

(1) Rubinstein, M.; Colby, R. H. *Polymer Physics*; Oxford University Press, 2003.

(2) Griffin, P. J.; Bocharova, V.; Middleton, L. R.; Composto, R. J.; Clarke, N.; Schweizer, K. S.; Winey, K. I. Influence of the Bound Polymer Layer on Nanoparticle Diffusion in Polymer Melts. *ACS Macro Lett.* **2016**, *5*, 1141–1145.

(3) Tonelli, A. E. Conformational Characteristics of Poly(2-Viny1pyridine). *Macromolecules* **1985**, *18*, 2579–2583.

(4) Park, J.; Bailey, E. J.; Composto, R. J.; Winey, K. I. Single-Particle Tracking of Nonsticky and Sticky Nanoparticles in Polymer Melts. *Macromolecules* **2020**, *53*, 3933–3939.

(5) Bailey, E. J.; Griffin, P. J.; Composto, R. J.; Winey, K. I. Multiscale Dynamics of Small, Attractive Nanoparticles and Entangled Polymers in Polymer Nanocomposites. *Macromolecules* **2019**, *52*, 2181–2188.